Crystal structure of bacterial multidrug efflux transporter AcrB

Satoshi Murakami*†§, Ryosuke Nakashima*, Eiki Yamashita‡ & Akihito Yamaguchi*†§

** Department of Cell Membrane Biology, Institute of Scientific and Industrial Research, Osaka University, Ibaraki, Osaka 567-0047, Japan*
† Faculty of Pharmaceutical Science, 1-6 Yamada-oka, Osaka University, Suita, Osaka 565-0871, Japan
‡ Institute for Protein Research, Osaka University, 3-2 Yamada-oka, Suita 565-0871, Japan
§ CREST, Japan Science and Technology Corporation, Osaka 567-0047, Japan

AcrB is a major multidrug exporter in *Escherichia coli*. It cooperates with a membrane fusion protein, AcrA, and an outer membrane channel, TolC. We have determined the crystal structure of AcrB at 3.5 Å resolution. Three AcrB protomers are organized as a homotrimer in the shape of a jellyfish. Each protomer is composed of a transmembrane region 50 Å thick and a 70 Å protruding headpiece. The top of the headpiece opens like a funnel, where TolC might directly dock into AcrB. A pore formed by three α-helices connects the funnel with a central cavity located at the bottom of the headpiece. The cavity has three vestibules at the side of the headpiece which lead into the periplasm. In the transmembrane region, each protomer has twelve transmembrane α-helices. The structure implies that substrates translocated from the cell interior through the transmembrane region and from the periplasm through the vestibules are collected in the central cavity and then actively transported through the pore into the TolC tunnel.

The emergence of bacterial multidrug resistance is an increasing problem in the treatment of infectious diseases. Multidrug resistance often results from the overexpression of a multidrug efflux system[1,2]. Genome sequence analysis of microorganisms has revealed the presence of several putative drug efflux transporter genes[3]. Among them, the AcrAB–TolC system is constitutively expressed in *E. coli* and is largely responsible for the intrinsic resistance of *E. coli* against dyes, detergents and most lipophilic antibiotics[4]. The AcrAB–TolC system is composed of a resistance-nodulation-cell division (RND)[5] transporter, AcrB, a membrane fusion protein (MFP)[6], AcrA, and a multifunctional outer membrane channel, TolC[7]; it transports a wide variety of noxious compounds from the cell directly into the medium, bypassing the periplasm[8,9]. The substrate specificity of the AcrAB system is unusually broad. It extrudes cationic, neutral and anionic substances[10].

In addition, the AcrAB system pumps out some β-lactams with multiple charged groups, which were experimentally shown not to traverse the cytoplasmic membrane. These substrates are thus likely to be captured from the periplasm[10]. The natural function of AcrAB is presumed to be the pumping out of bile salts and their derivatives to survive in the presence of the high concentrations of these detergents in the natural habitat of *E. coli*. AcrAB catalyses efflux driven by proton motive force; this has been experimentally proved in intact cells using uncouplers and ionophores[11], and also in reconstituted proteoliposomes using artificial proton motive force[9].

AcrB is the active part of the AcrAB–TolC drug export complex. It is composed of 1,049 amino-acid residues that form twelve putative

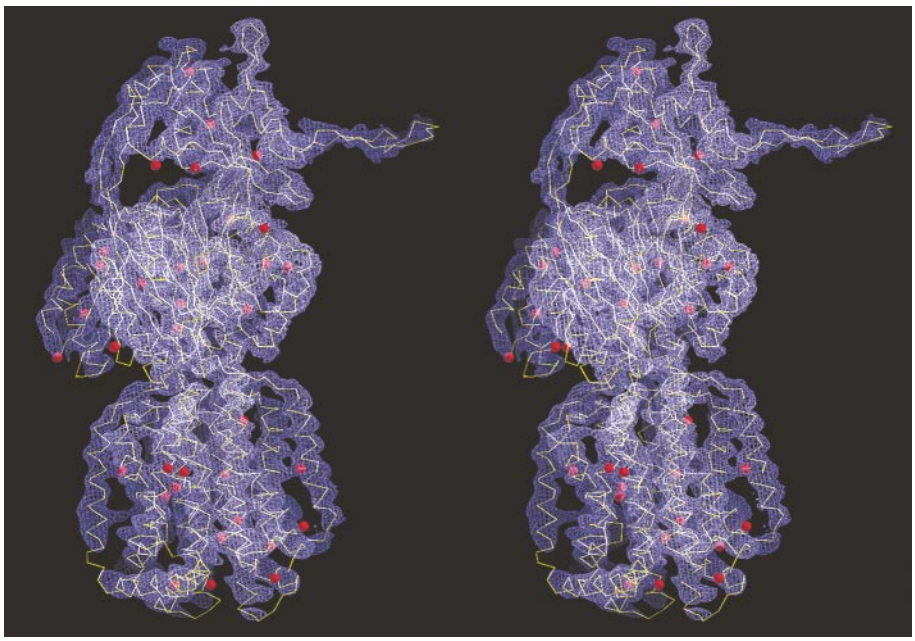

Figure 1 Stereo view of the experimental electron density map (2.0σ contoured, purple) of the AcrB protomer at 3.5 Å resolution. The Cα trace (yellow lines) is superimposed on the electron density map. This figure was prepared with program O (ref. 41). Thirty-eight selenium atoms are depicted as red balls.

transmembrane α-helices and two large hydrophilic loops on the periplasmic surface[12]. AcrA is an elongated molecule that is presumed to link or fuse the inner and outer membranes[13,14]. When engaged with its export substrate, AcrAB recruits TolC to form a transient complex that actively transports the substrates across both membranes. As shown in the crystal structure of TolC[15], it comprises a trimer with a characteristic 'channel-tunnel' structure composed of a porin-like outer-membrane channel 40 Å long connected with a cylinder[15] 100 Å long protruding into the periplasm.

Homologues of AcrB are widely distributed not only in Gram-negative bacteria but also in Gram-positive ones[5,16] and confer intrinsic drug tolerance to microorganisms. Also, mammalian cells have an RND-type transporter that plays an important physiological role. This protein, the Niemann–Pick C1, is responsible for the autosomal recessive disorder characterized by cholesterol accumulation in lysosomes. It has been identified as an RND permease that transports fatty acids from the endosome/lysosome system[17].

Recently, the crystal structures of ion-translocating membrane proteins such as K^+-channels[18] and Ca^{2+}-ATPases[19] were determined. The crystal structures of the lipid flippase MsbA[20] and the vitamin-B12-transporting ABC transporter[21] BtuCD of *E. coli* have also been reported. However, attempts to obtain high-resolution structures of the largest group of transport proteins, the proton-coupled secondary transporters, have been thus far unsuccessful. Electron microscopic analyses of several secondary transporters were recently reported[22–25]; however, the resolution was too low to assign helix-packing or to understand the mechanistic aspects of secondary transport.

Here, we determined the X-ray crystal structure of a secondary transporter AcrB, which exports a wide variety of organic compounds from the cell interior and also from the periplasm into the medium in combination with MFP and TolC. The structure of AcrB will greatly improve our understanding of the fundamental mechanism underlying active solute transport in general and multidrug transport in particular.

Structure determination

Initial phases at 4.3 Å were determined by the multiple isomorphous replacement (MIR) method using mercury, platinum and osmium derivatives. Out of 42 methionine residues, 38 sites were identified in the selenium anomalous difference Fourier map. MIR phases calculated by including selenomethionine-replaced crystal were extended to a 3.5 Å resolution by solvent flattening[26]. The backbone of the protein was successfully traced in the map as shown in Fig. 1 (see also Supplementary Fig. 1), and its amino-acid sequence was consistent with 38 selenomethionine sites and bulky electron-density contours of aromatic residues. A total of 1,006 amino acids out of 1,049 residues were located in the 3.5 Å map. Structure refinement by the program CNS reduced an R and R_{free} to 0.290 and 0.355, respectively. The main-chain dihedral angles for 70.6% of the non-glycine residues were in the most favoured region and only 0.5% of the non-glycine residues were in the disallowed regions of the Ramachandran plots[27]. The structural analysis is summarized in Table 1.

Overall architecture

AcrB comprises a trimer of 1,049-residue protomers (Fig. 2). The appearance of the trimer is that of a jellyfish with a three-fold symmetry axis perpendicular to the membrane plane. It comprises an extra-membrane (periplasmic) headpiece and a transmembrane region approximately 70 Å and 50 Å thick, respectively (Fig. 2a; see also Supplementary Information movie 1). The boundary of the membrane-embedded region (depicted as dotted lines in Fig. 2a) was estimated by the hydrophobic surface of the protein and the distribution of the aromatic amino acids. The maximum diameters of the headpiece and transmembrane region are approximately 100 Å and 80 Å, respectively. The headpiece is divided into two stacked parts. The upper and lower parts are 30 Å and 40 Å thick, respectively. The side view of the upper part has a trapezoidal appearance and is about 70 Å wide at the bottom and about 40 Å wide at the top. The crystal structure of TolC[15] indicates that it protrudes 100 Å into the periplasm. The sum of the periplasmic

Table 1 **Data collection and crystallographic analysis**

	Native	Derivatives			
		Hg	Pt	Os	Se
Space group	*R*32				
Wavelength (Å)	0.9000	0.9000	0.9000	0.9000	0.9795
Resolution (Å)	3.5 (3.63–3.5)	4.3 (4.45–4.3)	4.3 (4.45–4.3)	4.4 (4.56–4.4)	5.0 (5.1–5.0)
Observed reflections*	198,425 (13, 165)	102,662 (9,465)	87,755 (7,482)	96,176 (9,107)	131,081 (3,590)
Independent reflections	26,406 (2,584)	14,401 (1,406)	13,908 (1,393)	13,510 (1,338)	8,109 (720)
$I/\sigma(I)$	11.5 (2.6)	6.6 (5.4)	10 (6.5)	8.2 (5.0)	12.7 (6.9)
Averaged redundancy†	7.5 (5.1)	7.1 (6.7)	6.3 (5.3)	7.1 (6.8)	16.2 (5.0)
Completeness	98.8 (98.6)	99.7 (100)	94.9 (95.8)	99.3 (100)	87.9 (78.7)
R_{merge}‡	9.0 (36.5)	12 (30)	10.8 (24.6)	11.1 (39.2)	14.2 (33.2)
R_{iso}§		14.5	17.2	28.9	16.9
R_{cullis}‖		0.81	0.86	0.83	0.96
Phasing power¶		0.53	0.43	0.54	0.28
Overall figure of merit#			0.32		
Refinement					
Resolution range (Å)	8.0–3.5				
R factor (%)	29.0				
R_{free} (%)	35.5				
Bond length (Å)	0.0032				
Bond angles (degrees)	0.867				
Average *B*-factor for main-chain atoms (Å^2)	95				
Average *B*-factor for side-chain atoms (Å^2)	117				

All diffraction data used in this structural analysis were collected on BL44XU at SPring-8. All data were collected at 100 K.
*The numbers in parentheses are for the highest-resolution shells.
†Redundancy is the number of observed reflections for each independent reflection.
‡R_{merge}, $\sum_h\sum_i|I(h,i)-\langle I(h)\rangle|/\sum_h\sum_i I(h,i)$, where $I(h,i)$ is the intensity value of the ith measurement of h, and $\langle I(h)\rangle$ is the corresponding mean value of $I(h)$ for all i measurements; the summation is over the reflections with $I/\sigma(I)$ larger than 0.0.
§R_{iso}, $\sum|F_{PH}-F_P|/\sum F_{PH}$, where F_{PH} and F_P are the derivative and the native structure factor amplitudes, respectively.
‖R_{cullis}, $\sum||F_{PH}-F_P|-F_H(calc)|/\sum|F_{PH}-F_P|$, where F_H(calc) is the calculated heavy-atom structure factor. The summation is over the centric reflections only.
¶Phasing power is root-mean-square (r.m.s.) isomorphous difference divided by r.m.s. residual lack of closure.
#Figure of merit, $\langle|\sum P(\alpha)e^{i\alpha}/\sum P(\alpha)|\rangle$, where α is the phase and $P(\alpha)$ is the phase probability distribution.

length of AcrB and TolC is about 170 Å, which is enough to cross the periplasmic space. Given that the diameter of the top of the headpiece is almost equal to that of the TolC bottom[15], AcrB and TolC might be directly docked with each other. Thus, the domains of protomers forming the upper part are tentatively named TolC docking domains.

Viewed from the top, the upper part is open like a funnel (Fig. 2b; see also Supplementary Information movie 2). The internal diameter of the funnel opening is about 30 Å, which is consistent with that of the TolC conduit[15]. Three α-helices form a pore at the centre of the headpiece (Fig. 2b). Each protomer contributes one pore helix. The pore exists in the lower part of the headpiece and connects with the bottom of the funnel. The pore seems to be closed in the crystal structure, probably because it does not contain a bound substrate. The long hairpin structure (~35 Å) protrudes from the TolC docking domain of every protomer and inserts into that of the next protomer. This interlocking arrangement presumably provides a very strong interaction holding the headpiece together.

In contrast to the headpiece, the transmembrane domains of the protomers seem to be loosely packed. Three transmembrane domains of the protomers are arranged in a ring-like manner with a central hole (Fig. 2c). This hole crosses the membrane and extends to the bottom of the headpiece. The diameter of this hole is about 30 Å. It may be hard to keep phospholipids out of such a large transmembrane hole surrounded by the loosely interacting protomers. Thus, the transmembrane part of this hole might be filled with phospholipids.

Transmembrane domain structure

The transmembrane domain of each protomer contains twelve transmembrane α-helices (Fig. 2c). The number of the transmembrane segments is consistent with the hydropathy plot-based prediction and topology studies by site-directed chemical modification of cysteine mutants[12]. A pseudo-two-fold symmetry axis exists in each transmembrane domain, that is, the six N-terminal helices are symmetrically arranged with the six C-terminal helices. The root mean square (r.m.s.) difference value of the superimposition of Cα traces of the amino and carboxy-terminal halves of the transmem-

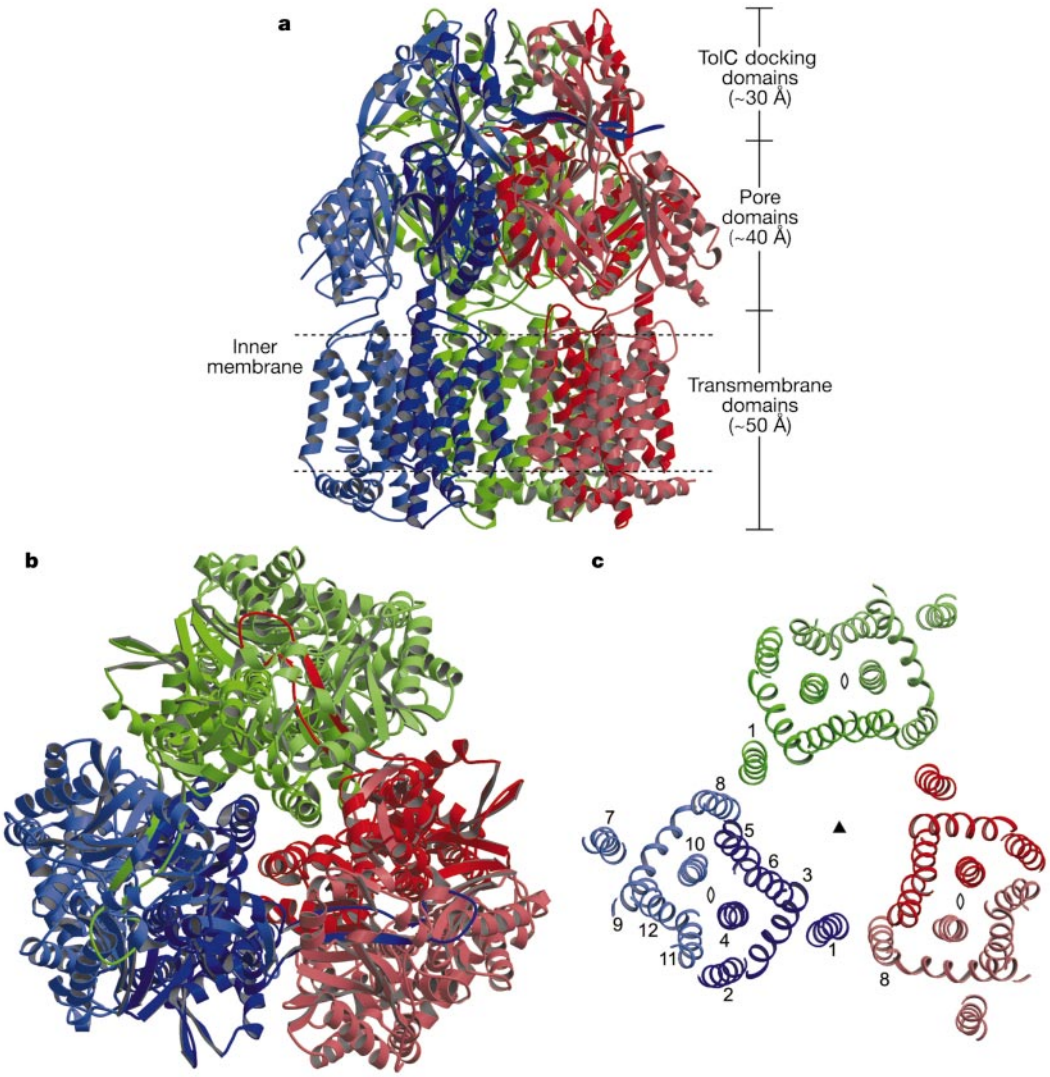

Figure 2 Structure of AcrB. **a**, Side view of a ribbon representation. Three protomers are individually coloured (blue, green and red). The N-terminal and C-terminal halves of the protomers are depicted as dark and pale colours, respectively. The extra-membrane (periplasmic) headpiece (TolC docking domains and pore domains) is at the top, and the transmembrane region is at the bottom. **b**, Top view of a ribbon representation. The protomers are individually coloured as in **a**. **c**, Structure within a slab (~23 Å) of the transmembrane domain parallel to the membrane plane near the periplasmic surface. The protomers are individually coloured as in **a** and **b**. Three-fold and pseudo-two-fold rotation axes are indicated. The label numbers indicate the transmembrane helix numbers (TMx in Fig. 3a). This figure, Fig. 3b and c, Fig. 4 and Fig. 5 were generated by MOLSCRIPT[43] and Raster3D[44].

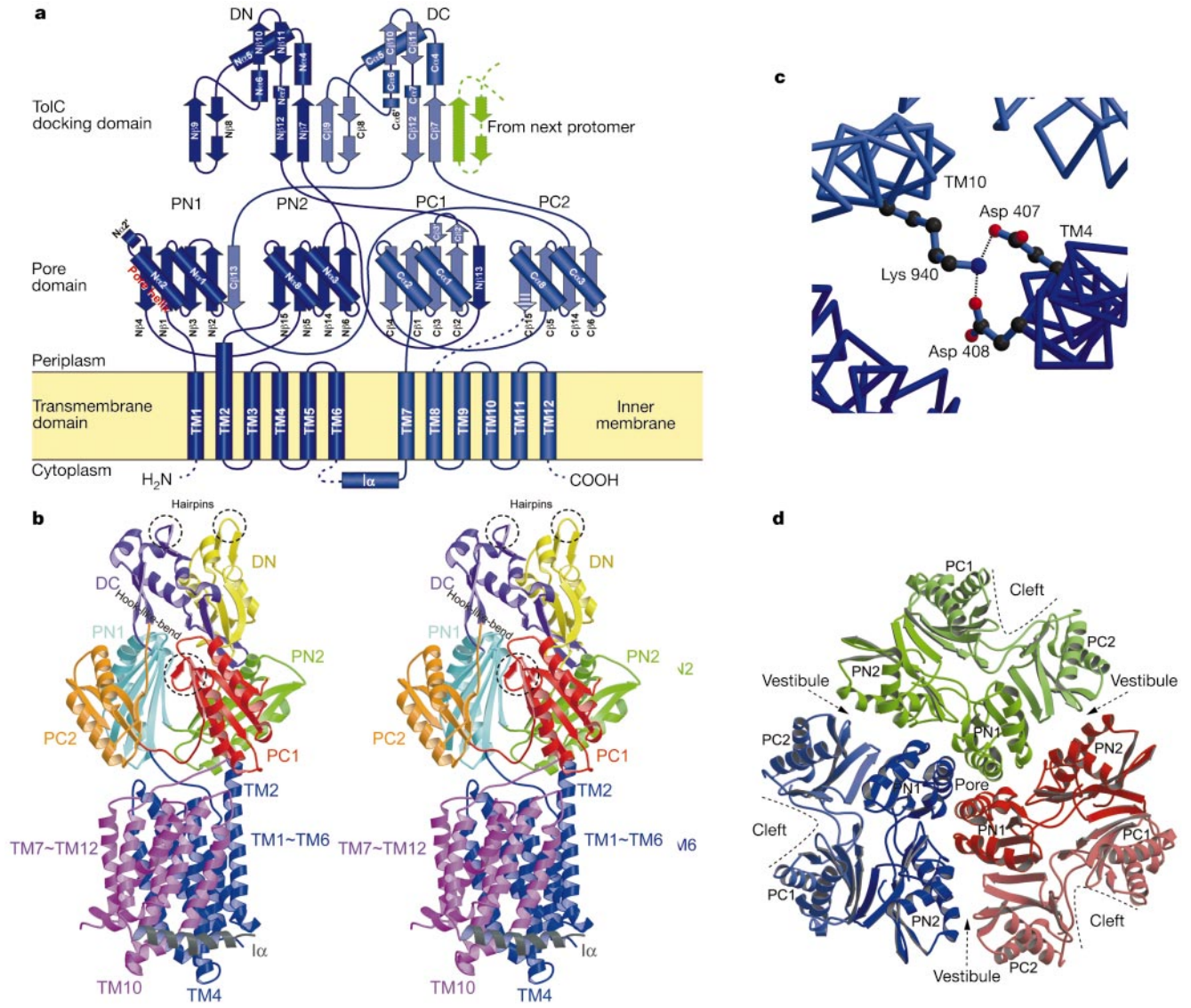

Figure 3 The structure of a single protomer. **a**, Topology diagram of the protomer. Secondary structure elements are indicated: TM, transmembrane helices; Nα and Nβ, helices and strands, respectively, in the N-terminal half of the headpiece; Cα and Cβ, helices and strands, respectively, in the C-terminal half of the headpiece; Iα, a helix attached to the cytoplasmic surface of the membrane. N- and C-terminal halves are depicted in dark and pale blue, respectively. Dotted lines depict disordered polypeptide segments, positions 1–6, 499–512, 711, 860–868 and 1,037–1,049. The pore domain (lower part of the headpiece) is divided into four subdomains, PN1, PN2, PC1 and PC2. The TolC-docking domain (upper part of the headpiece) is divided into two subdomains, DN and DC. The hairpin structure inserted into the TolC-docking domain from the next protomer is depicted in green. **b**, A stereo view of ribbon representation of a protomer viewed from outside the headpiece. Subdomains are depicted in different colours: PN1, cyan; PN2, green; PC1, red; PC2, orange; DN, yellow; DC, purple; N-terminal TM2, blue; C-terminal TM, magenta; Iα, grey. There is a cleft perpendicular to the membrane plane between PC1 and PC2. A short hairpin structure at the depth of the cleft is labelled 'Hook-like bend'. Two vertical hairpins at the top of DN and DC are depicted in dotted circles. **c**, Ion pairs between Asp 407, Asp 408 and Lys 940 in TM4 and TM10 at the view from the cytoplasmic side. Side chains of Asp 407, Asp 408 and Lys 940 are shown in ball-and-stick representation, with the positions of the C, N and O atoms indicated by grey, blue and red balls, respectively. **d**, Cut view of the pore domains from the boundary between the pore and TolC-docking domains.

brane domain is ~2.4 Å. The membrane domain contains an additional extra-membrane α-helix (Iα) located between TM6 and TM7 attached to the cytoplasmic membrane surface (Fig. 3a and b).

The inter-protomer interaction in the transmembrane region is restricted to the surface buried between TM1 and TM8 (Fig. 2c). TM4 and TM10 form the centre of the transmembrane helix bundle (Fig. 2c). These helices are long and protrude beyond the cytoplasmic surface of the membrane (Fig. 3b). TM2 is also a long helix that protrudes upwards across the boundary of the membrane (Fig. 3b). TM8 corresponds to TM2 in the C-terminal half. However, the polypeptide segment of the top of TM8 is disordered (amino-acid residues 860–868). Except for the asymmetry of the top of TM2 and TM8, pseudo-two-fold symmetry of the N- and C-terminal six-helix bundles can be observed in Fig. 2c.

According to the results of site-directed mutagenesis studies on MexB[28] and AcrB (A. Saito, N. Tamura, T. Hirata, S.M. and A.Y., unpublished work), the transmembrane region contains three functionally essential charged residues: Asp 407, Asp 480 and Lys 940. When these residues are replaced with any other amino-acid residues, the resulting mutants completely lose the drug resistance. These residues are located in the middle of TM4 and TM10, and form ion pairs (Fig. 3c). These residues are possible candidates for the proton-translocating pathway.

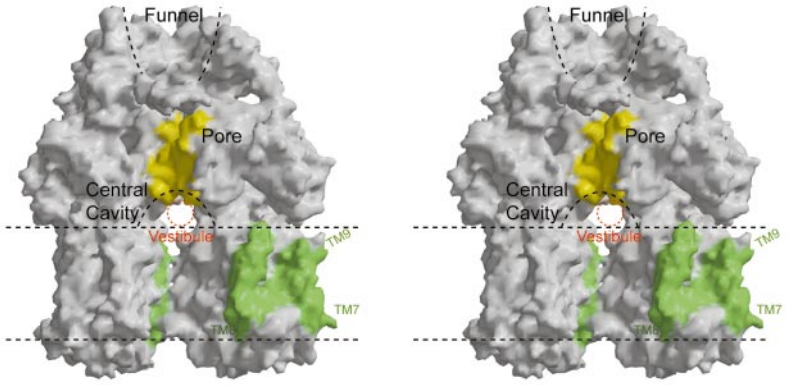

Figure 4 A cutaway stereo view displaying the solvent-accessible surface of AcrB rendered with GRASP[45]. The front protomer is removed. A hairpin inserted into the removed protomer is viewed at the upper left as a stick-like protuberance. A hole for insertion of a hairpin from the removed protomer is also viewed at the upper right. The yellow areas of the surface are coloured according to residues from Asp 99 to Leu 118 in pore helices (Nα2). The pale green areas are coloured according to residues in TM7 (Gly 539–Val 557) and TM8–TM9 (Ser 869–Phe 918). Frameworks of the funnel and the cavity are indicated by dotted lines.

Pore domain structure

The pore domain is composed of four subdomains: PN1, PN2, PC1 and PC2 (Fig. 3a and b). PN1 and PN2 comprise the polypeptide segment between TM1 and TM2, and PC1 and PC2 comprise the segment between TM7 and TM8. All of these subdomains contain a characteristic structural motif. That is, two β-strand–α-helix–β-strand motifs are directly repeated and sandwiched with each other. This motif forms a structure in which two α-helices are located on a four-stranded antiparallel β-sheet. As found by a database search (Dali/FSSP[29]), this motif also exists in carboxypeptidase G2 (ref. 30). In PN1 and PC1, there is an additional antiparallel β-strand from the other half of the protomer (Fig. 3a). Thus, the antiparallel β-sheets in PN1 and PC1 are composed of five β-strands. On the other hand, in PN2 and PC2, the repeat of the β–α–β motifs is interrupted by switching to the TolC docking domain, and PC1 and PN1, respectively (Fig. 3a). The exception of the topological symmetry in the pore domain is a short hairpin, Cβ2′–Cβ3′, and a short α-helix, Nα2′. The pore helix is an Nα2 in PN1 (Fig. 3a).

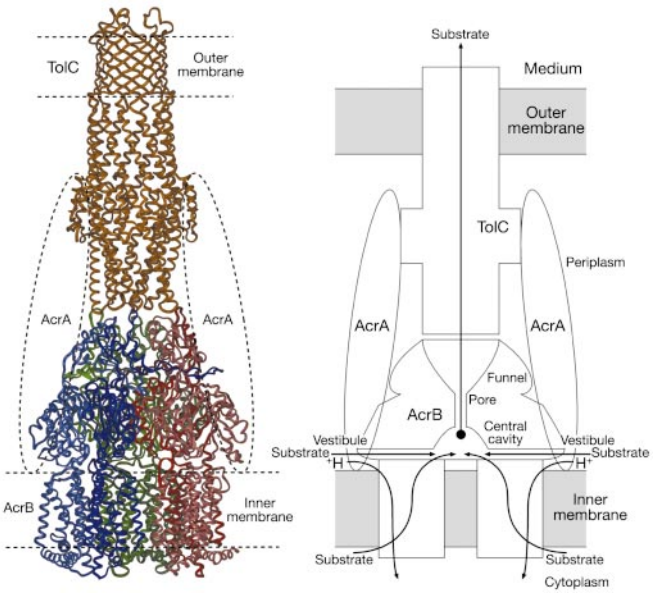

Figure 5 Proposed model of the AcrB–AcrA–TolC complex and the schematic mechanism of multidrug export mediated by AcrAB-TolC system. TolC structure[15] is manually docked to AcrB. Dotted ovals indicate AcrA molecules. This figure was produced using Insight II/Discover (Biosym/MSI).

Four subdomains in the pore domain are packed with their sheets back to back in the centre, placing the α-helices on the outside (Fig. 3b). The deep cleft perpendicular to the membrane plane exists between PC1 and PC2. Its length is approximately 40 Å, its width 20 Å and its depth 15 Å. The vertical cleft along to the outer surface of the headpiece might be a binding site for AcrA, which is estimated to have an elongated shape[13]. At the depth of the cleft, there is a short hairpin structure, Cβ2′–Cβ3′, in PC1, which forms a hook-like bend.

The lower part of the headpiece is composed of three pore domains, one for every protomer (Fig. 3d). The three pore domains combine to form a central pore in the headpiece. Viewed from the top, PN1, PN2, PC1 and PC2 are arranged in a clockwise order. PN1 is inside, and PN2, PC1 and PC2 are outside the headpiece (Fig. 3d). The pore-forming helix is the second helix (Nα2) of PN1. A cleft exists between PC1 and PC2 at the periphery of each protomer (Fig. 3d). Vestibules are open at the side of the headpiece between PN2 and PC2. They lead to a cavity located at the bottom of the pore as described below (Fig. 4).

TolC docking domain structure

The TolC docking domain is composed of two subdomains, DN and DC (Fig. 3a). Each subdomain contains a four-stranded mixed β-sheet. Two antiparallel β-strands are placed parallel to a hairpin structure from the other half or from the other protomer. The long hairpin structure (~35 Å) protrudes like a beak from subdomain DN (Fig. 3a; see also Supplementary Fig. 2). A vertical hairpin structure is located at the top of each subdomain of the TolC docking domain (Fig. 3a and b).

Three TolC docking domains form a funnel-like structure (Fig. 2b; see also Supplementary Information movie 2). The diameter of the top of the TolC docking domain is about the same as that of the bottom of TolC. The top of AcrB and the bottom of TolC fit well with each other by manual docking (Fig. 5; see also Supplementary Fig. 3). Six vertical hairpins, in total, at the top of AcrB trimer can contact with the six α-helix–turn–α-helix structures at the bottom of TolC[15] to form a tight seal, by inspection.

Proposed transport mechanism

Figure 4 shows a one-protomer cutaway stereo view displaying the solvent-accessible surface of AcrB. A stick-like protrusion from the upper left of the headpiece is a hairpin structure inserted into the front protomer, which has been removed. The hole at the upper right of the headpiece is for insertion of the hairpin structure from the removed protomer. The funnel opens widely at the top of the headpiece. The bottom end of the funnel is narrow and connects

with the pore. The proximal end of the pore connects a cavity which is an extramembrane part of the central transmembrane hole. If the hole is filled with phospholipids, the depth of the cavity between the end of the pore and the membrane plane is about 15 Å. These are vestibules open from the cavity into the periplasm at the side of the headpiece near the membrane plane. The vestibules exist between every protomer. Because a front protomer is removed from the trimer in Fig. 4, only one vestibule can be observed at the centre of the cavity, like a window open backward. Two other vestibules also exist in both sides of the cavity, although they are hardly distinguishable in Fig. 4. A substrate located on the membrane plane or in the outer leaflet of the membrane might gain access to the cavity through these vestibules.

There is a groove in the membrane-exposed peripheral surface of the transmembrane domain of each promoter between TM8 and TM7. It extends across the whole membrane-embedded surface (Fig. 4, green-coloured region). The bottom of the groove is formed by TM9. Because TM9 is tilted, the groove is shallow at the cytoplasmic end and deep at the periplasmic end. The top of this groove is connected with the cavity via the disordered region of the top of TM8. The disordered region is close to the vestibule. This groove might be a pathway for substrate translocation across the membrane. The shape of the groove (shallow at the cytoplasmic side and deep at the periplasmic side) suggests that the transport through this groove of substrates located in the inner leaflet of the membrane might be more favourable than those in the cytoplasm.

Our AcrB crystal structure provides a structural basis for considering the molecular mechanism of multidrug export. The structure is consistent with the possibility of a direct interaction between TolC and AcrB. When the substrate is transported, AcrB might recruit TolC to form a direct transit pathway from the cytoplasm to the extracellular milieu (Fig. 5). Two putative pathways for substrate entry into AcrB are seen (Fig. 5). Substrates located in the cytoplasm or inner leaflet of the membrane might be transported across the membrane through the transmembrane groove at the periphery of each transmembrane domain. Then, they might be collected in the central cavity. The possibility that substrates pass through the centre of each protomer cannot be ruled out, as the groove at the hydrophobic peripheral surface of the transmembrane domain seems to be favourable for amphiphilic substrates partitioned into the inner leaflet of the membrane. There is also a possibility that the trimer centre hole plays some role in the substrate translocation. However, this hole might be filled with phospholipids. Substrates located on the outer surface or in the outer leaflet of the membrane could gain access to the cavity through the vestibules open into the periplasm. They would then be actively transported through the pore into the TolC tunnel via the funnel. The ion pairs between Lys 940, Asp 407 and Asp 408 are possible candidates for the transmembrane proton translocation site. When these aspartic acids are protonated, the ion pairs are disrupted. The helices TM4 and TM10 may then undergo a conformational change. This conformational change may be transduced to the pore region by a remote conformational coupling and thereby open the pore.

The AcrAB–TolC system exports a wide variety of structurally unrelated compounds, most of which are amphiphilic[1,4]. In particular, the unique property of this system and other MFP-dependent systems, such as the MexAB–OprM in *Pseudomonas aeruginosa*, is its ability to confer resistance to β-lactam antibiotics[31,32]. The targets of the β-lactam antibiotics are periplasmic enzymes that participate in cell wall biosynthesis, and secondary transporters usually do not export solutes from the periplasm, so it has been surprising that RND transporters confer resistance to these drugs.

How do RND transporters actively export drugs from the periplasm? Nikaido *et al.* proposed a dual entrance model for the AcrB export mechanism; that is, substrates are taken up from the inner and outer leaflets of the lipid bilayer of the cell membrane[33]. However, there has been no experimental evidence for this model. In this regard, the crystal structure of AcrB provides a possible explanation. As shown, AcrB contains vestibules open to the periplasm at the side of the headpiece. They permit direct access of the substrates from the periplasm or outer leaflet of the membrane. AcrB can also mediate the translocation of the substrates from the cytoplasm or the inner leaflet of the membrane. This structure supports the dual-entrance model for AcrB-mediated multidrug export. □

Methods

Protein preparation

A histidine-tagged AcrB-overproducing plasmid pAcBH was previously constructed[12]. The AcrB was overproduced in *E. coli* JM109. The cells were disrupted with Microfluidizer M-110EH (Microfluidics Corp.) and the membrane fractions were collected and washed with several ultracentrifugation steps at 150,000*g* for 90 min. Purified membranes were resuspended in buffered glycerol (50 mM Tris-HCl, pH 7.0, 10% glycerol). Then membrane proteins were solubilized in 2% n-dodecyl-β-D-maltoside (DDM) (Anatrace). Lipids and debris were removed by ultracentrifugation at 170,000*g* for 60 min. Extracted histidine-tagged AcrB was purified with affinity column chromatography using Chelating Sepharose (Amersham Bioscience) immobilized with Ni^{2+} equilibrated with buffer (20 mM Tris-HCl, pH 7.5, 0.3 M NaCl, 10% glycerol and 0.2% DDM). The column was washd using 25 mM imidazole added to the above buffer and then 100 mM imidazole. Purified AcrB was eluted with 300 mM imidazole. Imidazole was removed by concentration-dilution steps of proteins three times on a ultrafiltration membrane. Proteins were finally concentrated to 35–40 mg ml^{-1}. For proteins labelled with seleno-1-methionine, transformed *E. coli* B834DE3 (Novagen, WI, USA) were grown in minimal medium (L-methionine was replaced by seleno-L-methionine), and the protein was purified as above. Replacement of methionine sulphur with selenium was confirmed by X-ray fluorescence analysis on BL44XU at SPring-8.

Preparation of native and derivative crystals

Crystals were grown by vapour diffusion from sitting drops at 25 °C. A protein solution containing 28 mg ml^{-1} histidine-tagged AcrB protein, 20 mM sodium phosphate (pH 6.2), 10% glycerol and 0.2% dodecylmaltoside was mixed (1:1) with a reservoir solution containing 15–16% polyethylene glycol 2000, 80 mM sodium phosphate (pH 6.2), 20 mM sodium citrate-HCl (pH 5.6). The crystals were grown within a few days to optimal size ($0.3 \times 0.3 \times 0.3$ mm^3). The concentration of glycerol was gradually increased from 5% to 30% in 5% steps by the soaking method for optimal cryo-protection. Crystals were picked up using nylon loops (Hampton Research) for flash-cooling in cold nitrogen gas from a cryostat (Rigaku, Japan) For derivatization, crystals were soaked for 1 h in cryo-protection buffer containing 0.5 mM K_2HgI_4, 1 mM K_2PtCl_6 and 1 mM $OsCl_3$ before freezing.

Crystallographic analysis

All data sets were collected on BL44XU at SPring-8 with imaging-plate detector DIP2040 (MAC-Science) at cryogenic temperature (100 K). The diffraction data were processed and scaled with DENZO and SCALEPACK[34], respectively. The native crystal belongs to the space group *R*32 with cell dimensions of $a = b = 144.3$ Å, $c = 519.0$ Å in the hexagonal setting. Three heavy-atom derivatives of mercury, osmium and platinum, and the seleno-methionine-replaced crystal were isomorphous with the native crystal. Initial phases were first calculated by program SOLVE[35] derived from the mercury derivative. The heavy-atom sites of the platinum and osmium derivatives were determined in difference Fourier maps calculated with the single isomorphous phases of the mercury derivative. MIR phase refinement with three heavy-atom derivatives was performed at 4.3 Å resolution with MLPHARE[36,37]. Anomalous dispersion effects of the heavy metals were taken into account for the phase estimation. To locate the methionine residues in the crystal, anomalous difference Fourier maps were calculated with coefficients of $(F_{Se}^{+} - F_{Se}^{-})\exp[i(\alpha_P - \pi/2)]$ at 5 Å resolution, where $(F_{Se}^{+} - F_{Se}^{-})$ was the Bijvoet difference of the selenomethionine-replaced crystal and where α_P was the MIR phase of the native crystal determined with the three derivatives. Out of 42 methionine sites of the protein molecule, 35 positions were identified by selenium peaks higher than 4σ, and 38 sites were higher than 3σ in the anomalous difference Fourier map. The selenomethionine-replaced crystal was included in MIR phases at 4.3 Å resolution. The phases were improved and extended to 3.5 Å resolution with RESOLVE[38,39]. Model building was performed using program O (ref. 40) and model refinement was conducted using Crystallographic and NMR system (CNS)[41]. Out of 1,049 residues of the whole molecule, the atomic parameters of residues 7–498, 513–710, 712–859 and 869–1,036 converged well during the refinement. A crystallographic R and an R_{free} for 5% reflections excluded from the refinement were reduced to 0.290 and 0.355, respectively. The refined structure was validated using the program PROCHECK[42]. The main-chain dihedral angles for 70.6% of the non-glycine residues were in the most favoured regions of the Ramachandran plots[27]: 26.3% in allowed regions; 2.6% in generously allowed regions; and 0.5% in the disallowed regions.

Received 17 May; accepted 6 August 2002; doi:10.1038/nature01050.

1. Okusu, H., Ma, D. & Nikaido, H. AcrAB efflux pump plays a major role in the antibiotic resistance phenotype of *Escherichia coli* multiple-antibiotic-resistance (Mar) mutants. *J. Bacteriol.* **178,** 306–308 (1996).
2. Ma, D., Cook, D. N., Hearst, J. E. & Nikaido, H. Efflux pumps and drug resistance in Gram-negative bacteria. *Trends Microbiol.* **2,** 489–493 (1994).

3. Paulsen, I. T., Nguyen, L., Sliwinski, M. K., Rabus, R. & Saier, M. H. Microbial genome analyses: comparative transport capabilities in eighteen prokaryotes. *J. Mol. Biol.* **301,** 75–100 (2000).
4. Sulavik, M. C. *et al.* Antibiotic susceptibility profiles of *Escherichia coli* strains lacking multidrug efflux pump genes. *Antimicrob. Agents Chemother.* **45,** 1126–1136 (2001).
5. Tseng, T.-T. *et al.* The RND permease superfamily: An ancient, ubiquitous and diverse family that includes human disease and development proteins. *J. Mol. Microbiol. Biotechnol.* **1,** 107–125 (1999).
6. Dinh, T., Paulsen, I. T. & Saier, M. H. Jr A family of extracytoplasmic proteins that allow transport of large molecules across the outer membrane of Gram-negative bacteria. *J. Bacteriol.* **176,** 3825–3831 (1994).
7. Paulsen, I. T., Park, J. H., Choi, P. S. & Saier, M. H. A family of Gram negative bacterial outer membrane factors that function in the export of proteins, carbohydrates, drugs, and heavy metals. *FEMS Microbiol. Lett.* **156,** 1–8 (1997).
8. Nikaido, H. How do exported proteins and antibiotics bypass the periplasm in Gram-negative bacterial cells? *Trends Microbiol.* **8,** 481–483 (2000).
9. Zguruskaya, H. I. & Nikaido, H. Bypassing the periplasm: Reconstitution of the AcrAB multidrug efflux pump of *Escherichia coli*. *Proc. Natl Acad. Sci. USA* **96,** 7190–7195 (1999).
10. Nikaido, H. & Zgurskaya, H. I. AcrAB and related multidrug efflux pumps of *Escherichia coli*. *J. Mol. Microb. Biotechnol.* **3,** 215–218 (2001).
11. Thanassi, D. G., Cheng, L. W. & Nikaido, H. Active efflux of bile salts by *Escherichia coli*. *J. Bacteriol.* **179,** 2512–2518 (1997).
12. Fujihira, E., Tamura, N. & Yamaguchi, A. Membrane topology of a multidrug efflux transporter, AcrB, in *Escherichia coli*. *J. Biochem.* **131,** 145–151 (2002).
13. Zgurskaya, H. I. & Nikaido, H. AcrA is a highly asymmetric protein capable of spanning the periplasm. *J. Mol. Biol.* **285,** 409–420 (1999).
14. Avila-Sakar, A. J. *et al.* Lipid-layer crystallization and preliminary three-dimensional structural analysis of AcrA, the periplasmic component of a bacterial multidrug efflux pump. *J. Struct. Biol.* **136,** 81–88 (2001).
15. Koronakis, V., Shaff, A., Koronakis, E., Luisi, B. & Hughes, C. Crystal structure of the bacterial membrane protein TolC central to multidrug efflux and protein export. *Nature* **405,** 914–919 (2000).
16. Poole, K. Multidrug efflux pumps and antimicrobial resistance in *Pseudomonas aeruginosa* and related organisms. *J. Mol. Microbiol. Biotechnol.* **3,** 255–264 (2001).
17. Davis, J. P., Chen, F. W. & Ioannou, Y. A. Transmembrane molecular pump activity of Niemann-Pick C1 protein. *Science* **290,** 2295–2298 (2000).
18. Doyle, D. A. *et al.* The structure of the potassium channel: molecular basis of K^+ conduction and selectivity. *Science* **280,** 69–77 (1998).
19. Toyoshima, T., Nakasako, M., Nomura, H. & Ogawa, H. Crystal structure of the calcium pump of sarcoplasmic reticulum at 2.6 Å resolution. *Nature* **405,** 647–655 (2000).
20. Chang, G. & Roth, C. B. Structure of MsbA from *E. coli*: A homolog of the multidrug resistance ATP binding cassette (ABC) transporters. *Science* **293,** 1793–1800 (2001).
21. Locher, K. P., Lee, A. T. & Rees, D. C. The *E. coli* BtuCD structure: A framework for ABC transporter architecture and mechanism. *Science* **296,** 1091–1098 (2002).
22. Williams, K. A. Three-dimensional structure of the ion-coupled transport protein NhaA. *Nature* **403,** 112–115 (2000).
23. Zhuang, J. *et al.* Two-dimensional crystallization of *Escherichia coli* lactose permease. *J. Struct. Biol.* **125,** 63–75 (1999).
24. Yin, C.-C. *et al.* The quaternary molecular architecture of TetA, a secondary tetracycline transporter from *Escherichia coli*. *Mol. Microbiol.* **38,** 482–492 (2000).
25. Heymann, J. A. W. *et al.* Projection structure and molecular architecture of OxlT, a bacterial membrane transporter. *EMBO J.* **20,** 4408–4413 (2001).
26. Wang, B. C. Resolution of phase ambiguity in macromolecular crystallography. *Methods Enzymol.* **115,** 90–112 (1985).
27. Ramakrishnan, C. & Ramachandran, G. N. Stereochemical criteria for polypeptide and protein chain conformations. II. Allowed conformations for a pair of peptide units. *Biophys. J.* **5,** 909–933 (1965).
28. Guan, L. & Nakae, T. Identification of essential charged residues in transmembrane segments of the multidrug transporter MexB of *Pseudomonas aeruginosa*. *J. Bacteriol.* **183,** 1734–1739 (2001).
29. Holm, L. & Sander, C. Mapping the protein universe. *Science* **273,** 595–602 (1996).
30. Rowsell, S. *et al.* Crystal structure of carboxypeptidase G2, a bacterial enzyme with applications in cancer therapy. *Structure* **5,** 337–347 (1997).
31. Srikumar, R., Li, X. Z. & Poole, K. Inner membrane efflux components are responsible for beta-lactam specificity of multidrug efflux pumps in *Pseudomonas aeruginosa*. *J. Bacteriol.* **179,** 7875–7881 (1997).
32. Mazzariol, A., Cornaglia, G. & Nikaido, H. Contributions of the AmpC beta-lactamase and the AcrAB multidrug efflux system in intrinsic resistance of *Escherichia coli* K-12 to beta-lactams. *Antimicrob. Agents Chemother.* **44,** 1387–1390 (2000).
33. Nikaido, H., Basina, M., Nguyen, V. Y. & Rosenberg, E. Y. Multidrug efflux pump AcrAB of *Salmonella typhimurium* excretes only those β-lactam antibiotics containing lipophilic side chains. *J. Bacteriol.* **180,** 4686–4692 (1998).
34. Otwinowski, Z. & Minor, W. Processing of X-ray diffraction data collected in oscillation mode. *Methods Enzymol.* **276,** 307–325 (1997).
35. Terwilliger, T. C. & Berendzen, J. Automated structure solution for MIR and MAD. *Acta Crystallogr. D* **55,** 849–861 (1999).
36. Otwinowski, Z. MLPHARE, CCP4 Proc. 80 (Daresbury Laboratory, Warrington, UK, 1991).
37. Collaborative Computational Project No. 4. The CCP4 suite: programs for protein crystallography. *Acta Crystallogr. D* **50,** 760–763 (1994).
38. Terwilliger, T. C. Maximum-likelihood density modification. *Acta Crystallogr. D* **56,** 965–972 (2000).
39. Terwilliger, T. C. Reciprocal-space solvent flattening. *Acta Crystallogr. D* **55,** 1863–1871 (1999).
40. Jones, T. A., Zou, J.-Y., Cowan, S. W. & Kjeldgaard, M. Improved methods for binding protein models in electron density maps and the location of errors in these models. *Acta Crystallogr. A* **47,** 110–119 (1991).
41. Brünger, A. T. *et al.* Crystallography & NMR system: A new software suite for macromolecular structure determination. *Acta Crystallogr. D* **54,** 905–921 (1998).
42. Laskowski, R. A., MacArthur, M. W., Moss, D. S. & Thornton, J. M. PROCHECK: a program to check the stereochemistry of protein structures. *J. Appl. Crystallogr.* **26,** 283–291 (1993).
43. Kraulis, P. J. MOLSCRIPT: a program to produce both detailed and schematic plots of protein structures. *J. Appl. Crystallogr.* **24,** 946–950 (1991).
44. Merritt, E. A. & Bacon, D. J. Raster3D: photorealistic molecular graphics. *Methods Enzymol.* **277,** 505–524 (1997).
45. Nicholls, A., Sharp, K. A. & Honig, B. Protein folding and association: insights from the interfacial and thermodynamic properties of hydrocarbons. *Proteins Struct. Funct. Genet.* **11,** 281–296 (1991).

Supplementary Information accompanies the paper on *Nature*'s website (**http://www.nature.com**).

Acknowledgements We thank T. Tsukihara for advice on all stages of our X-ray crystallographic analysis and critical reading of this manuscript, and M. Yoshida, H. Nikaido and E. Bibi for critical reading and discussions. We are also grateful to A. Nakagawa, M. Kusunoki and G. Kurisu for help in the diffraction data collection and computation. We thank D. Goodhew-Davison for English correction. This work was supported by Grants-in-Aid from the Ministry of Education, Culture, Sports, Science and Technology of Japan. This work was done with the approval of the Joint Research Committee of Institute for Protein Research, Osaka University.

Competing interests statement The authors declare that they have no competing financial interests.

Correspondence and requests for materials should be addressed to A. Y. (e-mail: akihito@sanken.osaka-u.ac.jp). Coordinates have been deposited with the Protein Data Bank under accession code 1IWG.